The Role of Internal Polarization and Electron Delocalization on Performance of Non-Fullerene Organic Solar Cells.

Qinghe Wu#[†◇], Donglin Zhao#[†], Matthew Goldey#[‡§], Alexander S. Filatov[†], Valerii Sharapov[†], Yamil Colon*[§], Zhengxu Cai[†], Xuanfeng Jiang[†], Junpeng Wang[†], Wei Chen[‡§], Juan de Pablo[‡§], Giulia Galli*[‡§] and Luping Yu*[†]

[†]Department of Chemistry and The James Franck Institute, The University of Chicago, 929 E 57th Street, Chicago, IL 60637

[◇]Department of Chemistry and Key Laboratory for Preparation and Application of Ordered Structural Materials of Guangdong Province, Shantou University, Guangdong 515063, P. R. China

[‡] Institute for Molecular Engineering and Materials Science Division, Argonne National Laboratory, 9700 Cass Avenue, Lemont, Illinois 60439, USA

[§]Institute for Molecular Engineering, the University of Chicago, 5747 South Ellis Avenue, Chicago, Illinois 60637, USA

@ Supporting Information

ABSTRACT: Two types of electron acceptors were synthesized by coupling two kinds of electron rich core with four equivalent PDI at α-position. The TPB and TPSe with π-orbitals spread continuously over the whole aromatic conjugated backbone; the TPC and TPSi contains isolated PDI units due to tetrahedron carbon or silicon linker. The calculations of the projected density of states (PDOS) show higher internal polarization and more extended intramolecular electron delocalization for TPB and TPSe than that for TPC and TPSi. The film absorption and emission spectra showed evidences for the intermolecular electron delocalization in TPB and TPSe, which are consistent with the network structure revealed by x-ray diffraction studies on single crystals of TPB. These features benefit the formation of charge transfer (CT) state and/or facilitate the charge transport. Thus, higher electron mobility and higher charge dissociation probabilities under J_{sc} condition were observed in blend films of TPB:PTB7-Th and TPSe:PTB7-Th than those in TPC:PTB7-Th and TPSi:PTB7-Th blend films. As a result, the J_{sc} and FF values of 15.02 mA/cm^2, 0.58 and 14.36 mA/cm^2, 0.55 for TPB and TPSe based solar cell are observed, while those for TPC and TPSi are 11.55 mA/cm^2, 0.47 and 10.35 mA/cm^2, 0.42, respectively.

Introduction

In the past several years, the rapid development of new electron acceptors has pushed the performance of non-fullerene OSC to the level that is comparable with or surpass that of fullerene OSC both in the individual parameters, such as fill factor (FF) and short circuit current (J_{sc}), and overall performance (PCE).[1-13] Among various electron acceptors, the compounds with an electron-rich core coupled with multiple electron-deficient moieties is very promising to replace expensive fullerene derivatives because of ease in synthesis and tunable optical/electronic properties.[14-29] In our previous communication, we reported development of an electron acceptor based on covalently bounded cluster of α-PDI (TPB), which was shown to exhibit an excellent organic photovoltaic properties.[18] To explain the interesting properties, a hypothesis was made that the built-in internal polarization and extended conjugation played important role in enhancing the OPV performances. It is well known that in bulky heterojunction solar cells, both donor and acceptor molecules absorb photons to generate excitons, which must undergo the exciton-dissociation at interfaces between electron donor and acceptor materials to form charge transfer (CT) state.[30,31] The Coulombically bound electron-hole pairs can further separate into free charges or relax back to the ground state via recombination.[32-35] It was shown that when donor polymers exhibited suitable internal polarization, efficient exciton-dissociation and charge separation can be achieved, leading to high performance of solar cell devices.[36-38] Our previous work indicated that internal polarization is equally important in designing electron acceptor.[18,39] To further provide firm evidence for this notion, in this paper, we studied two series of electron acceptors with different degree of molecular conjugation. The two series of molecules have marked differences in their optical and electronic properties, one with extended delocalization and internal polarization and another do not. The studies in solar cell performances, using PTB7-Th as donor polymer, showed that internal polarization and charge delocalization in electron acceptors influences charge dissociation and electron transporting, thus the corresponding OPV performance of non-fullerene solar cells.

It is also known that interpenetrating network of donor and acceptor molecules are crucial for charge transport in OPV devices. It was revealed that the ultrafast CT process and charge separation efficiency is strongly affected by the morphology and phase-separation structure in polymer/fullerene systems[40-42]. Revealing

charge separation process at donor/acceptor interface and investigating its relationship with chemical structure of donor and/or acceptor are crucial for rational design of semiconducting materials for OPV. Herein, we also report the crystal structure of the TPB molecule, which provide an opportunity to deduce structural information and better understanding of the OPV properties.

Result and discussion

Materials Design, Synthesis, and Electronic Properties previously, our group reported the enhanced OPV performance using acceptor with BDT-Th core coupled with four PDIs.[18,43] Herein, we designed and synthesized four compounds (Scheme 1) by employing two types of core linkers. One type core is BDT-Th and BDT-Se which have the π-orbitals spreading continuously over the whole conjugated backbone. The other type core is tetraphenylmethane (TBM) and tetraphenylsilane (TPS) which have the π-orbitals separated by a tetrahedron carbon and silicon center, respectively. The TPB and TPSe have the potential feature that allows each PDI to be conjugated through with the other three PDIs. The four PDIs in TPC and TPSi are all isolated by the tetrahedron carbon or silicon center.

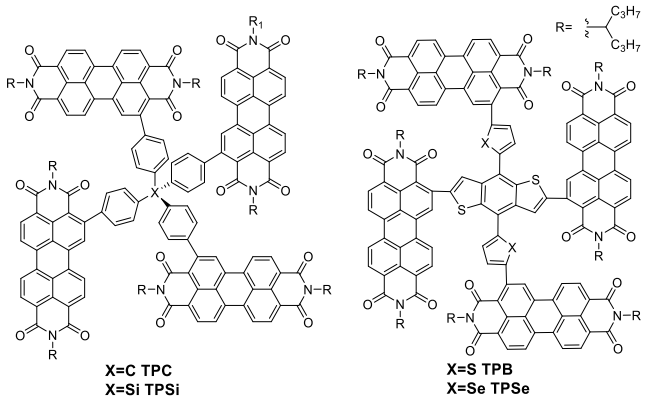

Scheme 1. Chemical structures of TPC, TPSi, TPB and TPSe.

These molecules (TPC, TPSi, TPB and TPSe) are synthesized via the Suzuki coupling reaction of tetra-pinacolatoboron-substituted BDT-Th/BDT-Se/TPM/TPS with four equivalents α-bromated PDIs in moderate yields with chemical structures showing in Scheme 1. All compounds show good solubility in common organic solvents such as methylene chloride, chloroform or chlorobenzene. Chemical structures of products were confirmed by ^{1}H NMR, mass spectroscopy and high-resolution mass spectroscopy.

Cyclic voltammetric measurements (CV) was used to determine the energy levels of four compounds, and the results are shown in Figure 2e,f. The TPC and TPSi exhibit the lowest unoccupied molecular orbital (LUMO) energy level of -3.75 and -3.77 eV, which are slightly higher than those for TPB and TPSe (-3.79 and -3.82 eV, respectively). The highest occupied molecular orbital (HOMO) energy level of both TPC and TPSi are -6.06 eV, which are slightly lower than those for TPB and TPSe (-5.94 and -5.97 eV, respectively). The LUMO energy level of the four compounds match well with that of PTB7-Th, with enough energy offset for electron transfer. However, HOMO energy level of four compounds is much lower than that of PTB7-Th.

Solar cell performance and active layer characterization Inverted solar cell devices with configuration of ITO/ZnO/Acceptor:PTB7-Th /MoO3/Ag were fabricated to evaluate photovoltaic properties of TPC, TPSi, TPB and TPSe. Active layers around 90 mn thick were deposited by spin-casting warm PTB7-Th:acceptor chlorobenzene solution. The optimized donor/acceptor ratio for four devices is all 1 to 1.5 in weight. No solvent additive is added in processing the film in the purpose of comparison. Typical current density-voltage (*J-V*) curves of the four devices are shown in Figure 1 and averaged parameters over 10 devices are summarized in Table 1. The devices based on TPB and TPSe exhibited the average power conversion efficiency (PCE) of 7.08 % and 6.36 %, while that for TPC and TPSi based solar cells is 4.60 % and 3.64 %. The trend is very clear that electron acceptors with better conjugation show higher photovoltaic properties than acceptors with isolated PDI units. The TPB and TPSe based solar cell devices exhibited higher FF and J_{sc} values. The J_{sc} and FF values are 15.02 mA/cm^2, 0.58 for TPB and 14.36 mA/cm^2, 0.55 for TPSe, while that for TPC and TPSi is 11.55 mA/cm^2, 0.47 and 10.35 mA/cm^2, 0.42, respectively. TPC and TPSi show slightly higher V_{oc} values than that for TPB and TPSe, that is consistent with variations in their LUMO energy level.

External quantum efficiency (EQE) spectra of the four devices are shown in Figure 1b. Integrated J_{sc} values from EQE spectrum are calculated to be 11.5 mA/cm^2 (TPC), 10.9 mA/cm^2 (TPSi), 14.1 mA/cm^2 (TPB) and 13.0 mA/cm^2 (TPSe). It should be noted that the J_{sc} values of TPC and TPSi devices integrated from EQE show negligible deviation from the J_{sc} values measured from *J-V* curves, while that for TPB and TPSe exhibit large negative deviation from *J-V* measurements. This is because TPB and TPSe based devices are found to suffer efficiency drop during UV-glue encapsulation procedure before devices are transferred out of glove box for EQE measurement.

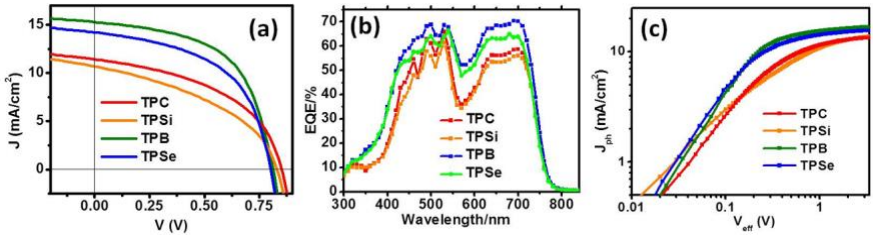

Figure 1. (a) *J-V* curves, (b) External quantum efficiency spectrum and (c) Photocurrent density (J_{ph}) versus effective voltage (V_{eff}) characteristics for solar cells with PTB7-Th as donor and TPC, TPSi, TPB or TPSe as acceptor.

Table 1. Device parameters of solar cell fabricated with PTB7-Th as donor and TPC, TPSi, TPB and TPSe as acceptors. Average data for over ten devices

Acceptor	J_{sc} (mA cm^{-2})	V_{oc} (V)	FF	Eff (%) (max)	□μ_h (cm^2/vs)	□μ_e (cm^2/vs)
TPC	11.55±0.15	0.85±0	0.47±0.00	4.60±0.04 (4.71)	4.0×10^{-4}	1.8×10^{-5}
TPSi	10.35±0.23	0.83±0	0.42±0.01	3.64±0.04 (3.68)	3.6×10^{-4}	1.4×10^{-5}
TPB	15.02±0.47	0.81±0	0.58±0.01	7.08±0.19 (7.38)	3.2×10^{-4}	9.1×10^{-5}
TPSe	14.36±0.26	0.81±0	0.55±0.01	6.32±0.25 (6.61)	3.0×10^{-4}	5.6×10^{-5}

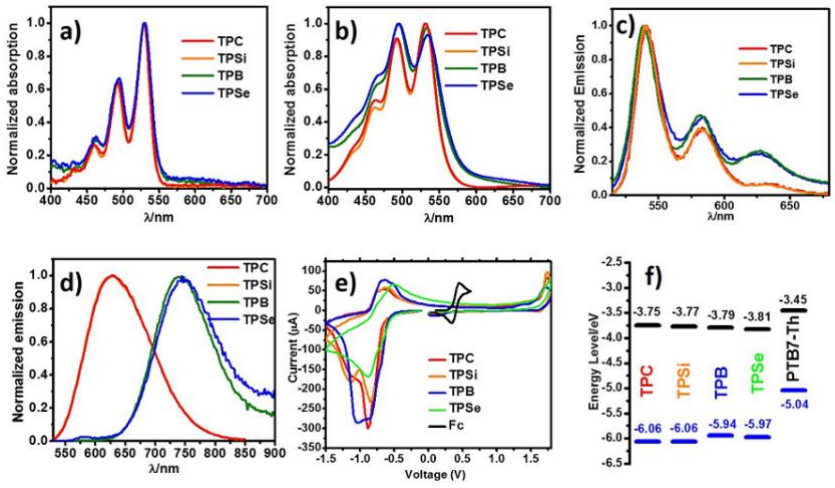

Figure 2 a) the solution and b) film absorption spectrum of TPC, TPSi, TPB and TPSe; c) the solution and d) film emission spectrum of TPC, TPSi, TPB and TPSe; e) cyclic voltammograms of TPC, TPSi, TPB and TPSe films with Fc/Fc$^+$ as the reference; f) Schematic of energy level of TPC, TPSi, TPB, TPSe and PTB7-Th.

Optical Properties. To explain the experimental results and gain deeper insight, optical absorption spectra of four compounds were investigated both in solution and films (Figure a, b). Solution absorption spectrums are taken in chlorobenzene at a concentration of 1.2×10^{-6} M. In solution, four acceptors show similar absorption with PDI monomer, three PDI characteristic peaks at 460, 495 and 530 nm, with intensity $I^{00}>I^{01}>I^{02}$. The absorption coefficients of the four compounds at maximum absorption are very similar, around 2.3×10^5 M^{-1}cm^{-1}. Comparedwith that of TPC and PTSi, the spectrum of TPB and TPSe exhibited a weak shoulder at 550-650 nm. Because the solution spectra were measured at very diluted solution, the absorption shoulder indicated an intramolecular D-A charge transfer state rather than the aggregation-induced feature, which indicated the internal polarization in compounds TPB and TPSe. The TPC and TPSi show similar film absorption as PDI monomer, the intensity of the three major transitions are still $I^{00}>I^{01}>I^{02}$. Onset of absorption is slightly redshifted from 550 nm to 569 nm. TPB and TPSe exhibit enhanced I01 and I02 absorption, with intensity of I01 exceeds I^{00}. Absorption onset is also redshifted from 553 nm to 584 nm. Both enhanced I^{01}/I^{00} value and larger red-shift of absorption onset imply TPB and TPSe have stronger electron coupling in solid state compared to TPC and TPSi.

Fluorescence emission of four compounds were measured both in 1.3 x 10^{-7} M dilute chlorobenzene solutions and films, excited at 495 nm. The TPC and TPSi exhibited relatively high emission quantum yield of 43 % and 15 % respectively, as measured by quanta-Q integration sphere. Fluorescence of TPB and TPSe are, however, largely quenched and too dim to be determined by integration sphere, which is caused by strong intramolecular charge transfer. Film fluorescence of TPC and TPSi exhibit a broad featureless peak with a maximum at 628 nm, while TPB and TPSe emission red shifted to 740 nm and 745 nm, respectively. The larger red shift of fluorescence of TPB and TPSe films indicates further extension of effective conjugation caused by strong intermolecular π-π interaction in solid states and excimer formation, which is the evidence of more delocalized electron wave function in TPB and TPSe films. The strong π-π intermolecular interaction is also

observed in TPB single crystal, discussed below. Thus, both intramolecular and intermolecular charge delocalization is more pronounced in compounds with conjugated core.

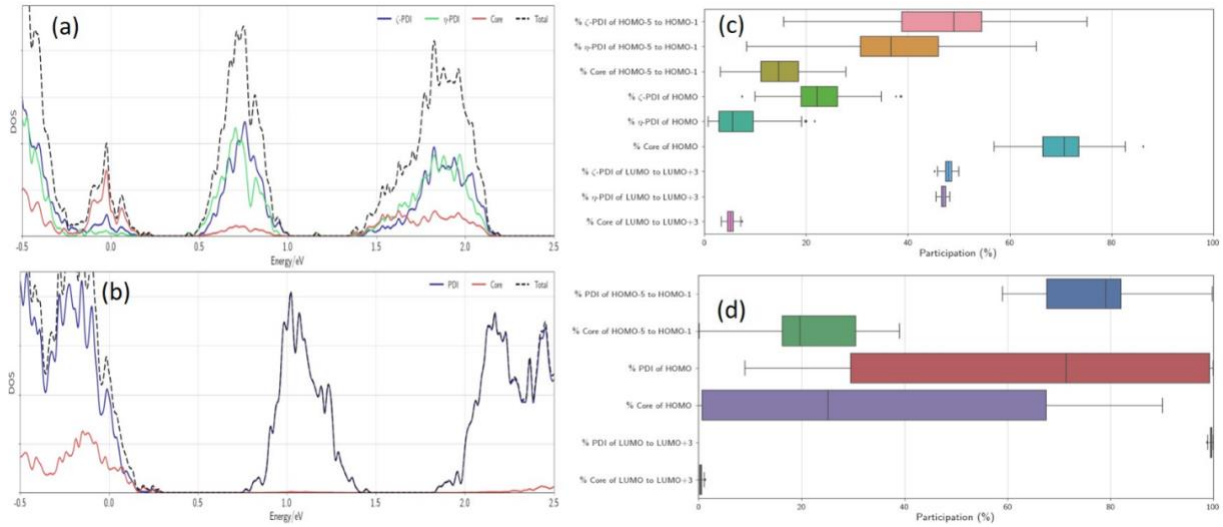

Figure 3a) Projected density of states for TPB with PDI attachments in the alpha position of the PDI bay. Core, ς-PDI, and η-PDI denote the bi-(thiophene)-benzodithiophene center, the PDIs directly attached to benzodithiophene(ς), and the PDIs attached to the core via thiophene(η), correspondingly. The zero of energy here is set to the valence band maximum. 3b) Projected density of states for TPC with PDI attachments in the alpha position of the PDI bay. Core and PDI denote the tetraphenyl carbon center and the attached PDIs, correspondingly. The zero of energy here is set to the valence band maximum. 3c) Participation of different chemical moieties of TPB in the $HOMO^{-5}$ to $HOMO^{-1}$ orbitals, the HOMO, and the LUMO to $LUMO^{+3}$ orbitals, as obtained from a projection onto atomic orbitals belonging to different moieties. Core, ς-PDI, and η-PDI denote the bi-(thiophene)-benzodithiophene center, the PDIs directly attached to benzodithiophene(ς), and the PDIs attached to the core via thiophene(η). Box widths denote the inner quartiles of the data, and whiskers denotes 1.5 times the quartiles. 3d) Participation of different chemical moieties in TPC in the $HOMO^{-5}$ to $HOMO^{-1}$ orbitals, the HOMO, and the LUMO to $LUMO^{+3}$ orbitals, as obtained from a projection onto atomic orbitals belonging to different moieties. Core and PDI denote the tetraphenyl carbon center and the attached PDIs. Box widths denote the inner quartiles of the data, and whiskers denotes 1.5 times the quartiles.

Electronic Structure Calculations. Detailed theoretical calculations also provided explanations for the above observations. Because of the similarity in chemical structure of TPB and TPSe, TPC and TPSi, only TPB and TPC were considered. Electronic structure calculations at the PBE level of theory were used for 133 (130) configurations of TPB (TPC) obtained from a glassy molecular dynamics snapshot after equilibrating a condensed phase simulation of pure TPB or TPC at 1000 K and cooling down to 400 K. Using a projected density of states (PDOS), averaged over molecular configurations, we identified differences in the DOS near the band edges, as shown in Figures 3a and 3b for TPB and TPC.

For both compounds, a four-fold degeneracy occurs at the conduction band minimum (CBM). For TPB, the valence band maximum (VBM) is isolated from other occupied states by 0.4 - 0.5 eV, which is distinct from TPC, where the VBM is nearly degenerate to a large manifold of states. The projection of the density of states onto the contributions from atomic orbitals within different chemical moieties is shown in Figures 3a and 3b, and box whisker plots of the contributions from different moieties within these compounds are shown in Figures 3c and 3d.

Projections of the energy levels onto atomic orbitals demonstrate very high participation of PDIs in the CBM for TPB (TPC) at 95±1 % (99.5±0.3 %) of the total PDOS. For TPB, where PDIs can be attached in two locations, PDIs attached via thiophene (denoted η) participate more in the CBM and VBM than PDIs attached directly to benzodithiophene (denoted ς). The remainder of the CBM stems from participation of the connective core of these compounds, which is 5±1 % (0.5±0.3 %) for TPB (TPC) of the total PDOS. The TPB VBM is dominated by core contributions (70±5 %), and it is qualitatively different from slightly deeper occupied states of TPB (where the core is 15±6 % of the $HOMO^{-5}$ to $HOMO^{-1}$ energy levels) and from the occupied manifold of TPC, where 34±32 % of the HOMO stems from the core. The large standard deviation of core contributions for TPC reflect the structural variety accessed within glassy phases and emphasizes the need for combining electronic structure and molecular dynamics studies of flexible, twisted multichromophores.

The calculated asymmetry in the core participation in TPB/TPC occupied and unoccupied states matches the B3LYP/6-31G* calculations, where HOMO electron density mainly localizes at BDT-Th core and the LUMO orbital mainly localizes at PDI unit for TPB[18], while both HOMO and LUMO orbital mainly localizes at PDI unit for TPC (Figure 4s). This result implies higher internal polarization of electron delocalization for TPB than that for TPC. Internal polarization enables electron-hole separation after photoexcitation. Due to the high participation of PDIs to the valence band maximum of TPC, dissociation of excitons into well-separated electron-hole pairs is expected to be less likely for TPC. The connective core participation in the CBM for TPB (5±1 %) is significantly higher than that (0.5±0.3 %) for TPC, indicating four PDIs in TPB are much more connected via LUMO orbital. Therefore, once an electron is obtained, the intramolecular electron delocalization should benefit charge separation. Since these molecules also have qualitative differences in the core participation

in the CBM, work is underway to predict how charge transport[44] in TPB and TPC varies with molecular configuration, and which structural features, such as linkage twisting[45], are strongly coupled to charge transport rates.

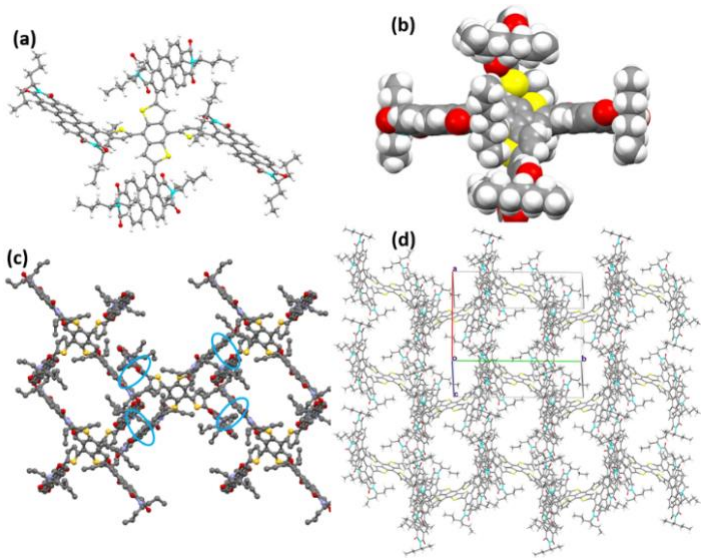

Figure 4. a) Side and b) top view of TPB single molecule; c) intermolecular packing along b and c axis, the intermolecular π-π interactions are marked with blue lines; d) 3D packing of TPB in single crystal.

Single crystal structure of TPB. To gain a better understanding of the three-dimensional packing of TPB molecules in the solid state, significant efforts were devoted to grow single crystals of this material. The TPB molecule is large (198 non-H atoms) and contains four PDI substituents connected via single bond linkages to the BDT-Th central unit. While crystallizing such a molecule posed a significant challenge, it was eventually found that TPB molecules can be grown into small single crystals by a very slow evaporation of its chloroform solution. The X-ray diffraction data were collected several times including two attempts using X-ray synchrotron radiation of the Advanced Photon Source at the Argonne National Lab (ChemMatCARS, Sector 15). Although best achieved results are still rather crude, the diffraction data allowed for a full resolution of all atoms and their refinement using isotropic thermal parameters (Figure 4a). In the molecule, the extended core is rather rigid and well resolved. Four PDI substituents form a cross-like molecular geometry with the angle of 75° between two mean planes passing through PDI subunits connected to thiophene substituents and two PDI subunits connected to BDT (Figure 4b). The dangling C7H15 alkyl side chains are extensively disordered due to high thermal motion as they located in the solvent filled voids. For refinement purposes, alkyl chains were introduced as fully constrained. The solvent accessible void volume of 5886 $Å^3$ (representing 1/2 of the unit cell volume of 11643 $Å^3$) and the electron count of 2074 electrons can account for 35 chloroform molecules crystallized in one-unit cell. It can be noted here that there are only three examples of single crystal structural analysis carried out with the same BDT-Th substituted core[46-48] and only one of them is of comparable complexity to the structure reported here.

The obtained single crystal structure provides interesting structural insight into the charge transport pathway. The crystal packing is dominated by π-stacking between the individual PDI moieties (Figure 4c). All four PDIs are involved in intermolecular interactions with an inter-plane separation starting at ca. 3.3 Å. These interactions lead to the formation of infinite 2D sheets. Dangling alkyl side chains along with the solvent media fill the space between the sheets. Such strong π-π intermolecular interactions may represent charge carriers transporting channels[49] facilitating the electron delocalization over more TPB molecules. This is consistent with the observation in film absorption and emission spectrum. Thus, it can be proposed that when TPB is mixed with polymers, a continuous charge transport pathway can be established via intermolecular π-π interactions and intramolecular BDT linkage. This should be in contrast with those of TPC and TPSi.

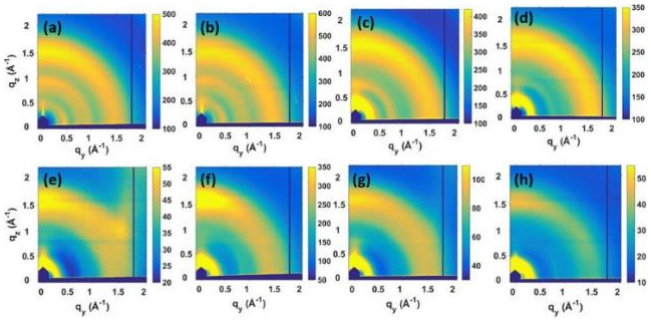

Figure 5. 2D GIWAXS patterns of films on ZnO-modified Si substrates. a) neat TPC film; b), neat TPSi film; c), neat TPB film; d), neat TPSe film; e), blend film of TPC:PTB7-Th; f), blend film of TPSi:PTB7-Th; g), blend film of TPB:PTB7-Th; h), blend film of TPC:PTB7-Th.

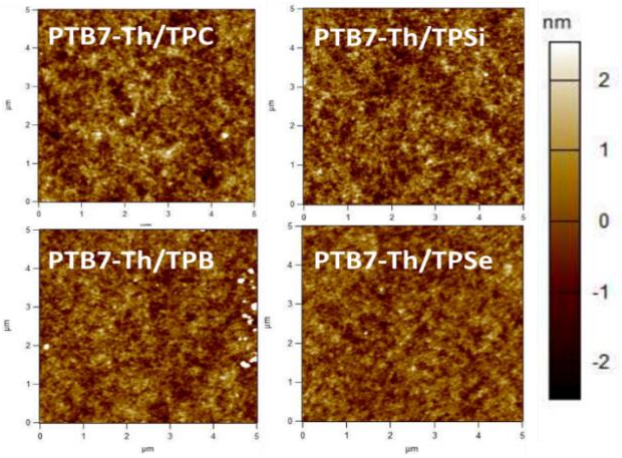

Figure 6. AFM of films of a) TPC:PTB7-Th; a) TPSi:PTB7-Th; a) TPB:PTB7-Th and a) TPSe:PTB7-Th.

Active layer Characterization. Both GIWAXS and AFM studies offer not much insight about the blend film structures. The 2D GIWAXS patterns are shown in Figure 5 and the out-of-plane/in-plane line cuts from GIWAXS patterns are exhibited in Figure S2. Although the GIWAXS pattern of TPC, TPSi, TPB and TPSe neat films show three low-intensity arc-shapes scattering, indicating weak crystalline nature and molecular orientation isotropy for all four compounds. The four blend films show similar features, where the scattering peaks due to small molecule acceptors all merge with that of donor polymer. The films topography (Figure 6) of four blend films from the atomic force microscopy (AFM) studies are all smooth with surface roughness value of between 0.5 and 0.6 nm, and show very similar topographic feature, which do not account for their OPV performance variation. This characteristic of non-fullerene BHJ blend film poses challenge in morphological studies due to their lack of contrast.

Charge carrier mobility. Electron and hole mobility were measured in four devices. The four blend films exhibited similar hole mobility, calculated to be 4.0×10^{-4} cm^2/vs for TPC:PTB7-Th, 3.6×10^{-4} cm^2/vs for TPSi:PTB7-Th, 3.2×10^{-4} cm^2/vs for TPB:PTB7-Th and 3.0×10^{-4} cm^2/vs for TPSe:PTB7-Th, respectively. Large differences were observed in the electron mobility, which reflects the property of the acceptor molecule. The TPC and TPSi blend films have low electron mobility of 1.8×10^{-5} cm^2/vs and $1.4\times10^{-5}cm^2/vs$. The TPB and TPSe blend films show higher mobility values of 9.1×10^{-5} cm^2/vs and 5.6×10^{-5} cm^2/vs, clearly due to intramolecular conjugation and network due to strong intermolecular π-π stacking. The higher electron mobility is beneficial to FF values, thus PCE values.

Exciton dissociation and charge generation. The structural differences in electron delocalization of these acceptors were also manifested in their changes in saturation current density (J_{sat}) and charge dissociation probabilities $P(E,T)$ of devices in combination with PTB7-Th. The J_{sat} will only be limited by total amount of absorbed incident photons if all the photogenerated excitons are dissociated into free charge carriers and collected by electrodes at a high V_{eff} (i.e. V_{eff} = 2.5 V). Here, photocurrent density (J_{ph}) is defined as $J_{ph} = J_L - J_D$, where J_L and J_D are the current densities under illumination and dark, respectively. Effective voltage (V_{eff}) is defined as $V_{eff} = V_0 - V_{app}$, where $V0$ is the voltage where J_{ph} equals zero and V_{app} is applied bias voltage. Figure 2c illustrates characteristic curves of J_{ph} versus V_{eff} for the four devices. The J_{sat} values varied for the four devices from 13.18 mA cm^{-2} (TPC), 13.31 mA cm^{-2} (TPSi), 16.59 mA cm^{-2} (TPB) to 15.41 mA cm^{-2} (TPSe), respectively. The results suggested that photogeneration of charge is more efficient in TPB and TPSe devices than those in TPC and TPSi devices. The $P(E, T)$ values calculated by normalizing J_{ph} with J_{sat} for the four devices under short circuit condition were 85 % (TPC), 78 % (TPSi), 92 % (TPB) and 92 % (TPSe), respectively. It is clear that acceptors with conjugated cores (TPB and TPSe) exhibit more efficient exciton dissociation and charge generation inside solar cell devices because the delocalization of electron wave-function facilitate charge transfer (CT) state overcoming coulombical attraction and resulting in higher J_{sc} values.[34,35] As shown in theoretical calculation of TPC, the high participation of PDIs to the valence band maximum, dissociation of excitons into well-separated electron-hole pairs is expected to be less likely for TPC than those in TPB system that are polarized.

Conclusion

Two types of electron acceptors were synthesized by coupling two kinds of electron rich core with four equivalent PDI at □-position. Comprehensive studies indicated that the TPB and TPSe with π-orbitals spread continuously over the whole aromatic conjugated backbone exhibit higher electron mobility and higher charge dissociation probabilities under J_{sc} condition, thus higher solar cell performances than that the TPC and TPSi containing isolated PDI units due to tetrahedron carbon or silicon linker. These results show the importance of internal polarization and electron delocalization in non-fullerene acceptor materials.

ASSOCIATED CONTENT

The supporting information is available. It includes synthesis, absorption spectra, photoluminescence spectra, theoretical calculation and device fabrication and characterization. "CCDC 1551964 contains the supplementary crystallographic data for this paper. The data can be obtained free of charge from The Cambridge Crystallographic Data Centre via www.ccdc.cam.ac.uk/structures."

AUTHOR INFORMATION

Corresponding author: lupingyu@uchicago.edu; gagalli@uchicago.edu.

Author contribution: # Authors made equal contribution.

ACKNOWLEDGMENT

This work was supported by NIST via CHIMAD program (QHW, MG, YC, JDP, GG and LPY). DOE via the ANSER Center, an Energy Frontier Research Center funded by the U.S. Department of Energy, Office of Science, Office of Basic Energy Sciences, under award number DE-SC0001059 (VS) and U. S. National Science Foundation grant (DLZ, NSF DMR-1263006) and NSF MRSEC program at the University of Chicago (WYL, DMR- 1420709). W.C. gratefully acknowledges financial support from the US Department of Energy, Office of Science, Materials Sciences and Engineering Division. Use of the Advanced Photon Source (APS)

at the Argonne National Laboratory was supported by the US Department of Energy, Office of Science, Office of Basic Energy Sciences, under Contract No. DE-AC02-06CH11357. ChemMatCARS Sector 15 is principally supported by the Divisions of Chemistry (CHE) and Materials Research (DMR), National Science Foundation, under grant number NSF/CHE-1346572. Use of the Advanced Photon Source, an Office of Science User Facility operated for the U.S. Department of Energy (DOE) Office of Science by Argonne National Laboratory, was supported by the U.S. DOE under Contract No. DE-AC02-06CH11357.

REFERENCES

(1) Bin, H. J.; Zhang, Z. G.; Gao, L.; Chen, S. S.; Zhong, L.; Xue, L. W.; Yang, C.; Li, Y. F. *J Am Chem Soc* **2016**, *138*, 4657.
(2) Holliday, S.; Ashraf, R. S.; Wadsworth, A.; Baran, D.; Yousaf, S. A.; Nielsen, C. B.; Tan, C. H.; Dimitrov, S. D.; Shang, Z. R.; Gasparini, N.; Alamoudi, M.; Laquai, F.; Brabec, C. J.; Salleo, A.; Durrant, J. R.; McCulloch, I. *Nature Communications* **2016**, *7*.
(3) Meng, D.; Fu, H. T.; Xiao, C. Y.; Meng, X. Y.; Winands, T.; Ma, W.; Wei, W.; Fan, B. B.; Huo, L. J.; Doltsinis, N. L.; Li, Y.; Sun, Y. M.; Wang, Z. H. *J Am Chem Soc* **2016**, *138*, 10184.
(4) Zhong, Y.; Trinh, M. T.; Chen, R.; Purdum, G. E.; Khlyabich, P. P.; Sezen, M.; Oh, S.; Zhu, H.; Fowler, B.; Zhang, B.; Wang, W.; Nam, C.-Y.; Sfeir, M. Y.; Black, C. T.; Steigerwald, M. L.; Loo, Y.-L.; Ng, F.; Zhu, X. Y.; Nuckolls, C. *Nature communications* **2015**, *6*, 8242.
(5) Jing Liu, S. C., Deping Qian, Bhoj Gautam, Guofang Yang, Jingbo Zhao,; Jonas Bergqvist, F. Z., Wei Ma, Harald Ade, Olle Ingan, Kenan Gundogdu,; Feng Gao, H. Y. *Nature Energy* **2016**, *1*, 1*7.
(6) Zhao, W. C.; Qian, D. P.; Zhang, S. Q.; Li, S. S.; Inganas, O.; Gao, F.; Hou, J. H. *Adv Mater* **2016**, *28*, 4734.
(7) Nikolka, M.; Nasrallah, I.; Rose, B.; Ravva, M. K.; Broch, K.; Sadhanala, A.; Harkin, D.; Charmet, J.; Hurhangee, M.; Brown, A.; Illig, S.; Too, P.; Jongman, J.; McCulloch, I.; Bredas, J. L.; Sirringhaus, H. *Nature Materials* **2017**, *16*, 356.
(8) Liu, F.; Zhou, Z. C.; Zhang, C.; Vergote, T.; Fan, H. J.; Liu, F.; Zhu, X. Z. *J Am Chem Soc* **2016**, *138*, 15523.
(9) Chen, S. S.; Liu, Y. H.; Zhang, L.; Chow, P. C. Y.; Wang, Z.; Zhang, G. Y.; Ma, W.; Yan, H. *J Am Chem Soc* **2017**, *139*, 6298.
(10) Lu, L.; Zheng, T.; Wu, Q.; Schneider, A. M.; Zhao, D.; Yu, L. *Chemical Reviews* **2015**, *115*, 12666.
(11) Zhao, W. C.; Li, S. S.; Yao, H. F.; Zhang, S. Q.; Zhang, Y.; Yang, B.; Hou, J. H. *J Am Chem Soc* **2017**, *139*, 7148.
(12) Liu, Y. H.; Zhang, Z.; Feng, S. Y.; Li, M.; Wu, L. L.; Hou, R.; Xu, X. J.; Chen, X. B.; Bo, Z. S. *J Am Chem Soc* **2017**, *139*, 3356.
(13) Kan, B.; Feng, H. R.; Wan, X. J.; Liu, F.; Ke, X.; Wang, Y. B.; Wang, Y. C.; Zhang, H. T.; Li, C. X.; Hou, J. H.; Chen, Y. S. *J Am Chem Soc* **2017**, *139*, 4929.
(14) Zhan, C. L.; Yao, J. N. *Chem Mater* **2016**, *28*, 1948.
(15) Li, Y. X.; Zhong, L.; Wu, F. P.; Yuan, Y.; Bin, H. J.; Jiang, Z. Q.; Zhang, Z. J.; Zhang, Z. G.; Li, Y. F.; Liao, L. S. *Energ Environ Sci* **2016**, *9*, 3429.
(16) Zhong, H. L.; Wu, C. H.; Li, C. Z.; Carpenter, J.; Chueh, C. C.; Chen, J. Y.; Ade, H.; Jen, A. K. Y. *Adv Mater* **2016**, *28*, 951.
(17) Lin, Y. Z.; Zhao, F. W.; He, Q.; Huo, L. J.; Wu, Y.; Parker, T. C.; Ma, W.; Sun, Y. M.; Wang, C. R.; Zhu, D. B.; Heeger, A. J.; Marder, S. R.; Zhan, X. W. *J Am Chem Soc* **2016**, *138*, 4955.
(18) Wu, Q. H.; Zhao, D. L.; Schneider, A. M.; Chen, W.; Yu, L. P. *J Am Chem Soc* **2016**, *138*, 7248.
(19) Hwang, Y. J.; Li, H. Y.; Courtright, B. A. E.; Subramaniyan, S.; Jenekhe, S. A. *Adv Mater* **2016**, *28*, 124.
(20) Lee, J.; Singh, R.; Sin, D. H.; Kim, H. G.; Song, K. C.; Cho, K. *Adv Mater* **2016**, *28*, 69.
(21) Liu, Y.; Mu, C.; Jiang, K.; Zhao, J.; Li, Y.; Zhang, L.; Li, Z.; Lai, J. Y. L.; Hu, H.; Ma, T.; Hu, R.; Yu, D.; Huang, X.; Tang, B. Z.; Yan, H. *Adv Mater* **2015**, *27*, 1015.
(22) Zheng, Y.-Q.; Dai, Y.-Z.; Zhou, Y.; Wang, J.-Y.; Pei, J. *Chem Commun* **2014**, *50*, 1591.
(23) Nielsen, C. B.; Holliday, S.; Chen, H. Y.; Cryer, S. J.; McCulloch, I. *Accounts Chem Res* **2015**, *48*, 2803.
(24) Wang, S. T.; Wang, M.; Zhang, X.; Yang, X. D.; Huang, Q. L.; Qiao, X. L.; Zhang, H. X.; Wu, Q. H.; Xiong, Y.; Gao, J. H.; Li, H. X. *Chem Commun* **2014**, *50*, 985.
(25) Kwon, O. K.; Park, J.-H.; Park, S. K.; Park, S. Y. *Adv Energy Mater* **2015**, *5*.
(26) Hartnett, P. E.; Matte, H. S. S. R.; Eastham, N. D.; Jackson, N. E.; Wu, Y. L.; Chen, L. X.; Ratner, M. A.; Chang, R. P. H.; Hersam, M. C.; Wasielewski, M. R.; Marks, T. J. *Chemical Science* **2016**, *7*, 3543.
(27) Wang, K.; Firdaus, Y.; Babics, M.; Cruciani, F.; Saleem, Q.; El Labban, A.; Alamoudi, M. A.; Marszalek, T.; Pisula, W.; Laquai, F.; Beaujuge, P. M. *Chem Mater* **2016**, *28*, 2200.
(28) Li, M. M.; Liu, Y. T.; Ni, W.; Liu, F.; Feng, H. R.; Zhang, Y. M.; Liu, T. T.; Zhang, H. T.; Wan, X. J.; Kan, B.; Zhang, Q.; Russell, T. P.; Chen, Y. S. *J Mater Chem A* **2016**, *4*, 10409.
(29) Zhao, D.; Wu, Q.; Cai, Z.; Zheng, T.; Chen, W.; Lu, J.; Yu, L. *Chem Mater* **2016**, *28*, 1139.
(30) Camaioni, N.; Po, R. *J Phys Chem Lett* **2013**, *4*, 1821.
(31) Clarke, T. M.; Durrant, J. R. *Chemical Reviews* **2010**, *110*, 6736.
(32) Stoltzfus, D. M.; Donaghey, J. E.; Armin, A.; Shaw, P. E.; Burn, P. L.; Meredith, P. *Chemical Reviews* **2016**, *116*, 12920.
(33) Wang, T.; Kafle, T. R.; Kattel, B.; Chan, W. L. *J Am Chem Soc* **2017**, *139*, 4098.
(34) Hartnett, P. E.; Mauck, C. M.; Harris, M. A.; Young, R. M.; Wu, Y. L.; Marks, T. J.; Wasielewski, M. R. *J Am Chem Soc* **2017**, *139*, 749.
(35) Yang, B.; Yi, Y. P.; Zhang, C. R.; Aziz, S. G.; Coropceanu, V.; Bredas, J. L. *J Phys Chem C* **2014**, *118*, 27648.
(36) Lu, L. Y.; Yu, L. P. *Adv Mater* **2014**, *26*, 4413.
(37) Carsten, B.; Szarko, J. M.; Lu, L. Y.; Son, H. J.; He, F.; Botros, Y. Y.; Chen, L. X.; Yu, L. P. *Macromolecules* **2012**, *45*, 6390.
(38) Carsten, B.; Szarko, J. M.; Son, H. J.; Wang, W.; Lu, L. Y.; He, F.; Rolczynski, B. S.; Lou, S. J.; Chen, L. X.; Yu, L. P. *J Am Chem Soc* **2011**, *133*, 20468.
(39) Jung, I. H.; Lo, W. Y.; Jang, J.; Chen, W.; Zhao, D. L.; Landry, E. S.; Lu, L. Y.; Talapin, D. V.; Yu, L. P. *Chem Mater* **2014**, *26*, 3450.
(40) Jakowetz, A. C.; Bohm, M. L.; Zhang, J. B.; Sadhanala, A.; Huettner, S.; Bakulin, A. A.; Rao, A.; Friend, R. H. *J Am Chem Soc* **2016**, *138*, 11672.
(41) Vandewal, K.; Himmelberger, S.; Salleo, A. *Macromolecules* **2013**, *46*, 6379.
(42) Huang, Y.; Kramer, E. J.; Heeger, A. J.; Bazan, G. C. *Chemical Reviews* **2014**, *114*, 7006.
(43) Wu, Q. H.; Zhao, D. L.; Yang, J. H.; Sharapov, V.; Cai, Z.; Li, L. W.; Zhang, N.; Neshchadin, A.; Chen, W.; Yu, L. P. *Chem Mater* **2017**, *29*, 1127.
(44) Goldey, M. B.; Brawand, N. P.; Voros, M.; Galli, G. *J Chem Theory Comput* **2017**, *13*, 2581.
(45) Goldey, M. B.; Reid, D.; de Pablo, J.; Galli, G. *Physical Chemistry Chemical Physics* **2016**, *18*, 31388.
(46) Jiang, Y.; Cabanetos, C.; Allain, M.; Liu, P.; Roncali, J. *Tetrahedron Lett* **2015**, *56*, 2324.
(47) Sun, K.; Xiao, Z. Y.; Lu, S. R.; Zajaczkowski, W.; Pisula, W.; Hanssen, E.; White, J. M.; Williamson, R. M.; Subbiah, J.; Ouyang, J. Y.; Holmes, A. B.; Wong, W. W. H.; Jones, D. J. *Nature Communications* **2015**, *6*.
(48) Bin, H. J.; Gao, L.; Zhang, Z. G.; Yang, Y. K.; Zhang, Y. D.; Zhang, C. F.; Chen, S. S.; Xue, L. W.; Yang, C.; Xiao, M.; Li, Y. F. *Nature Communications* **2016**, *7*.
(49) Dong, H.; Fu, X.; Liu, J.; Wang, Z.; Hu, W. *Adv Mater* **2013**,

25, 6158.

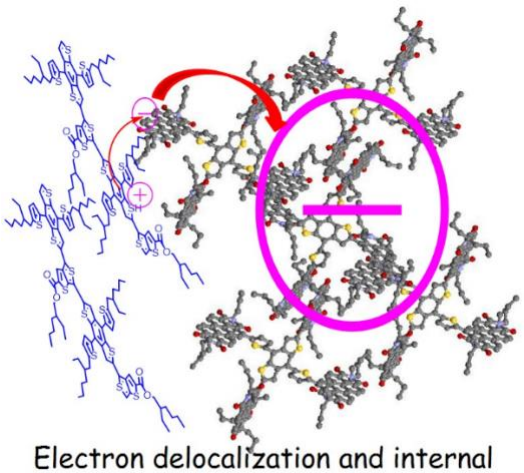
Electron delocalization and internal
polarization benefit charge separation!